Anthropogenic changes in the Walker circulation and their impact on the extra-tropical planetary wave structure in the Northern Hemisphere

Reindert J. Haarsma · Frank Selten

Abstract A robust change in the tropical circulation induced by anthropogenic warming in CMIP3 models is a weakening of the Walker circulation. This weakening affects the upper tropospheric divergence thereby modifying the propagation of Rossby waves from the tropics into the extra-tropics. It can be modeled by the barotropic vorticity equation forced with a Rossby wave source that is computed from the upper tropospheric divergence. Using the BVE as a diagnostic tool it is demonstrated for the CMIP3 models that the weakening of the Walker circulation has a significant impact on the extra-tropical planetary wave structure and to a large extent explains the projected changes in the mid tropospheric meridional wind in the CMIP3 models. The dominant response is a wave number five pattern similar to the circumglobal waveguide pattern. This analysis implies that a correct simulation of the Walker circulation and its response to anthropogenic changes are crucial for a correct simulation of the anthropogenic change in the extra-tropical planetary wave structure. Structure and intensity of the Walker circulation of the CMIP3 models show significant deviations from the Walker circulation as diagnosed from the ERA-interim and NCEP/NCAR reanalysis. Improving the simulation of the Walker circulation is a prerequisite to narrow the uncertainty in the projected anthropogenic change in the extra-tropical planetary wave structure.

Keywords Climate change · Planetary wave structure · Atmospheric dynamics · Walker circulation

R. J. Haarsma (✉) · F. Selten
Royal Netherlands Meteorological Institute (KNMI),
P.O. Box 201, 3730 AE De Bilt, The Netherlands
e-mail: haarsma@knmi.nl

1 Introduction

In the extra-tropics the regional impact of anthropogenic warming is predominantly affected by the change in the structure of the large scale planetary waves. The position and amplitude of the planetary waves modify the large scale atmospheric surface circulation, temperature distribution and precipitation patterns. Anthropogenic climate projections differ substantially with respect to the simulated change in the planetary wave structure (van Ulden and van Oldenborgh 2006; Déqué et al. 2007). This hampers the possibility to produce reliable climate projections. A better understanding of the basic mechanisms that govern the anthropogenic change in the planetary wave structure is therefore crucial for more reliable projections of regional anthropogenic climate change.

As discussed by Woollings (2010) in a review article "there have been surprisingly few studies attempting to interpret climate model projections from the perspective of the stationary waves". Stephenson and Held (1993) and Joseph et al. (2004) analyzed the stationary wave response using a linear steady state model. Recently Brandefelt and Körnich (2008) used a linear barotropic model to investigate the impact of the change in the zonal state on the planetary wave structure. These studies point towards different mechanisms affecting the planetary wave structure. Brandefelt and Körnich (2008) and Joseph et al. (2004) indicate the change of the zonal mean state as the dominant cause of the change in the planetary wave structure, whereas Stephenson and Held (1993) found that this was primarily due to changes in latent heat and transient eddy forcing.

An important source of interannual variability of extra-tropical planetary waves resides in the tropics. Tropical variability affects the extra-tropical atmospheric circulation

due to the generation of equivalent barotropic Rossby waves that propagate from the tropics into the extra-tropics (Hoskins and Karoly 1981; Held and Kang 1987; Hoskins and Ambrizzi 1993). Given the importance of the tropics for the interannual variability of the extra-tropical planetary waves it is natural to investigate the role of the tropics in explaining the anthropogenic change of the planetary wave structure.

One of the more robust changes in the tropical circulation induced by anthropogenic warming in CMIP3 models is a weakening of the Walker circulation. The physical cause of this weakening has been discussed by Vecchi and Soden (2007) and Held and Soden (2006). The weakening has also already been observed from data (Vecchi et al. 2006). Figure 1 shows for a set of CMIP3 models (described in Table 1) the monthly mean of the change in the area averaged value of the zonally asymmetric part of the absolute value of the tropical divergence at 300 hPa under an SRES A1B scenario. All models show a significant decrease indicating a weakening of the Walker circulation. The magnitude of decrease varies among the different models but is on average around 20–30% by the end of this century. This is a substantial decrease and we hypothesize that it will significantly affect the generation of Rossby waves propagating into the extra-tropics and impact the extra-tropical planetary wave structure.

The propagation of Rossby waves from the tropics into the extra-tropics is to first order adequately modeled by the barotropic vorticity equation (BVE), forced by an anomalous Rossby wave source (RWS) (Sardeshmukh and Hoskins 1985). The contributions to the anomalous RWS consist of vortex stretching (compression) due to tropical upper tropospheric divergence (convergence) and the advection of tropical upper tropospheric vorticity by the anomalous divergent wind. The RWS is computed for the upper troposphere which is the region of maximum divergence (convergence). Because the extra-tropical response is to a large extend equivalent barotropic changes in the upper tropospheric RWS affect the extra-tropical planetary wave structure over the entire height of the troposphere and can be modeled effectively by the BVE. An outstanding example of the successful application of the BVE is the explanation of the impact of El-Niño (Held and Kang 1987; Haarsma and Opsteegh 1989) on the extra-tropical circulation. Also the anthropogenic response of the planetary wave structure in the extra-tropics is predominantly barotropic as illustrated in Fig. 2, displaying the change in the 200 and 500 hPa streamfunction for one member of the ESSENCE simulations (see Sect. 3). This motivated us to use the BVE for investigating the impact of anthropogenic changes in the Walker circulation on the extra-tropical planetary wave structure.

Here we will use the BVE to improve our understanding of the anthropogenic change in the planetary wave structure in comprehensive CMIP3 climate models (Meehl et al. 2007) as used in the IPCC AR4 report (Solomon et al. 2007). It is used as a diagnostic tool to investigate the impact of the change in the Walker circulation on the planetary wave structure in those models.

The BVE and how it will be used to analyze the impact of the tropics on the extra-tropical planetary wave structure will be described in Sect. 2. Section 3 describes the climate model data that we have analyzed. The results of the analysis are given in Sect. 4, followed by a discussion in Sect. 5 and the conclusions in Sect. 6.

Fig. 1 Time evolution of the monthly mean of the absolute value of the divergence $(10^{-6}\ s^{-1})$ averaged at 300 hPa over the tropical band between 20°S and 20°N for CMIP3 models. The *different colors* indicate the CMIP3 models described in Table 1
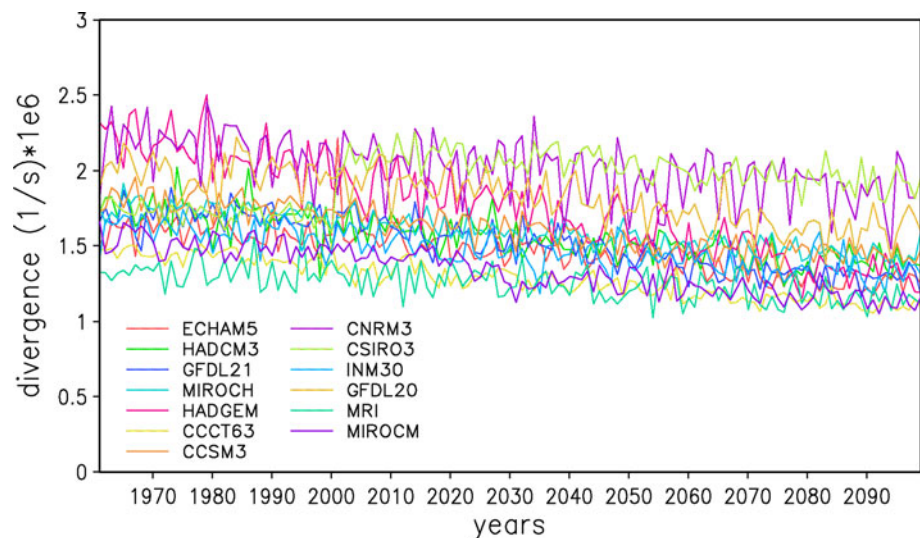
Table 1 CMIP3 models that have been analyzed

Model name	Short name	Originating	Country	Atmospheric
CCSM3.1	CCSM3	NCAR	USA	T85, L26
CGCM3.1 (T63)	CCCT63	CCCMA	Canada	T63, L31
CNRM-CM3	CNRM3	Met-France/CNRM	France	T63, L45
CSIRO-Mk3.0	CSIRO3	CSIRO	Australia	T63, L18
ECHAM5/MPI-OM	ECHAM5	MPI	Germany	T63, L31
GFDL-CM2.0	GFDL20	GFDL	USA	2.5×2, L24
GFDL-CM2.1	GFDL21	GFDL	USA	2.5×2, L24
INM-CM3.0	INM30	INM	Russia	5×4, L21
MIROC3.2 (hires)	MIROCH	CCSR, NIES, FRCGC	Japan	T106, L56
MIROC3.2 (medres)	MIROCM	CCSR, NIES, FRCGC	Japan	T42, L20
MRI-CGCM2.3.2	MRI	MRI	Japan	T42, L30
UKMO-HadCM3	HADCM3	UKMO	UK	3.75×2.5, L19
UKMO-HadGEM	HADGEM	UKMO	UK	1.875×1.25, L38

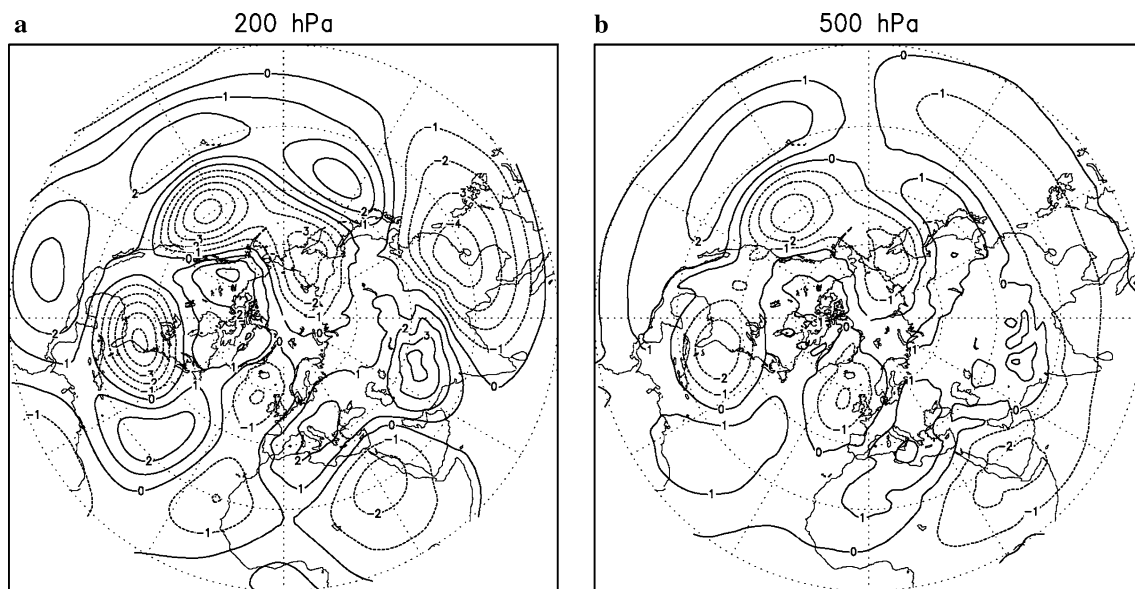More information is available online (http://www-pcmdi.llnl.gov)

Fig. 2 Change in streamfunction (*contour* interval 10^6 m^2 s^{-1}) at 200 hPa (**a**) and 500 hPa (**b**) between 2071–2100 and 1971–2000 for member 1 of the ESSENCE ensemble. The zonal mean average has been subtracted

2 Barotropic vorticity equation and Rossby wave source

The BVE including Ekman friction, dissipation and forcing is given by:

$$\frac{\partial \xi}{\partial t} + J(\psi, \xi + f) + \varepsilon \xi + \alpha \nabla^2 \xi = F$$

where ξ is relative vorticity, ψ streamfunction and $f = 2\Omega \sin \varphi$ the coriolis parameter. F denotes the forcing. The third and fourth term of the l.h.s. represent Ekman friction and dissipation respectively. The values for the Ekman friction ε and dissipation α will be chosen such that the solution of the BVE is marginally stable. Time integrations will then converge to a single stable solution. The topography is not explicitly included in the Jacobian J, but implicitly incorporated in the forcing term F. The BVE will be used to investigate and understand the simulated changes in the extra-tropical planetary wave structure by general circulation models (GCMs), in particular those generated by changes in the tropical circulation. We will focus here on the simulated long term mean anthropogenic changes. It implies that we assume stationary solutions:

$$\frac{\overline{\partial \xi}}{\partial t} = 0$$

where the overbar denotes the long term (30-year) mean. The forcing F_p that produces this long term mean for the Present climate can be computed from the long term mean simulated by the GCM

$$F_p = J(\overline{\psi_p, \xi_p + f}) + \varepsilon \overline{\xi_p} + \alpha \nabla^2 \overline{\xi_p}.$$

where the subscript p indicates the Present climate. Similarly for the Future climate

$$F_f = J(\overline{\psi_f, \xi_f + f}) + \varepsilon \overline{\xi_f} + \alpha \nabla^2 \overline{\xi_f}$$

where the subscript f indicates the Future climate. $\Delta F = F_f - F_p$ is the difference between Present and Future forcing. The difference in the tropical zonally asymmetrical forcing is given by

$$\Delta F_{asym}^{trop} = \Delta F^{trop} - [\Delta F^{trop}]$$

where the brackets indicate zonal averaging. The tropics are defined here as the region between 30°S and 30°N.

Alternatively, in the tropics changes in F can be approximated by changes in the RWS S (Sardeshmukh and Hoskins 1985):

$$S = -\bar{\varsigma}\bar{D} - \vec{V}_\chi \cdot \nabla\bar{\varsigma} = -\nabla \cdot (\vec{V}_\chi \bar{\varsigma})$$

where $\zeta = \xi + f$ is absolute vorticity and D divergence. The divergent wind $\vec{V}_\chi = -\nabla\chi$, where χ is the velocity potential. The first term of the RWS is vortex stretching (compression) and the second the advection of vorticity by the divergent wind. A first order approximation of the RWS is $-fD$.

The dynamics of the extra-tropical planetary waves is best simulated by the BVE if it is applied at the equivalent barotropic level, which according to Haltiner (1971) is at about 500 hPa, although Held et al. (1985) indicate a slightly higher level of 425 hPa. The forcing of Rossby waves in the tropics occurs, however, on a much higher level at about 200 hPa, where the divergence has its maximum amplitude (see Fig. 3 below). The baroclinic structure of Rossby waves in the tropics transforms into an equivalent barotropic structure by vertical mixing and downward propagation, when they travel into the extra-tropics. Because our focus is on the dynamics of Rossby waves in the extra-tropics we apply the BVE at equivalent barotropic level, which we choose here at 500 hPa. The RWS is, on the other hand, computed at 200 hPa, where the Rossby waves in the tropics are forced.

If the BVE is able to simulate to first order the tropical origins of the anthropogenic changes in the planetary wave structure then ΔF_{asym}^{trop} and the change in the RWS $\Delta S = S_f - S_p$ should be similar.

The BVE is solved on the sphere by a spectral model at triangular truncation T21 (Verkley 1987). The time scale of Ekman friction is 10 days. The time scale of the diffusion for the smallest horizontal scale is 4 days. For these values the 30 year mean climatology is marginally stable. Sensitivity experiments demonstrated that the results are not very sensitive to the choice of these values. The model is run to a stationary equilibrium in 2 years.

3 Data and model simulations

We have analyzed the output of the CMIP3 models using the SRES A1B scenario. The models and the simulations that are used are described in Table 1. In the choice of the available CMIP3 models we were guided by van Ulden and van Oldenborgh (2006). Only those models that have, according to the metric of van Ulden and van Oldenborgh (2006), a positive annual skill in mean sea level pressure for the Northern Hemisphere were included. We will refer to the periods 1971–2000 and 2071–2100 as Present and Future respectively. To give all CMIP3 models the same weight we included only one member of each CMIP3 model in case more members were available.

In addition we have analyzed the climate change simulations of the ECHAM5/MPI-OMI model used in the ensemble experiment ESSENCE (Sterl et al. 2008). This is a 17 member ensemble also using the SRES A1B scenario. The large ensemble enables a clear separation between internal variability and the mean anthropogenic response. The code of ECHAM5/MPI-OMI model in ESSENCE is the same as the CMIP3 ECHAM5 model in Table 1. Similar as for the CMIP3 models we will refer to periods 1971–2000 and 2071–2100 as Present and Future respectively.

For comparison with observations we have used the ERA40 (Uppala et al. 2005), ERA-interim (Dee et al. 2011) and NCEP/NCAR reanalysis (Kalnay et al. 1996).

We have used monthly mean data to compute seasonal means for December–January–February (DJF) and analyzed the data for the Northern Hemisphere. Climatological seasonal means were computed for the Present and Future periods. The choice for DJF is motivated by the fact that the impact of the tropical forcing on the Northern Hemisphere planetary wave structure is largest during boreal winter. During boreal summer the upper tropospheric easterlies block the propagation of Rossby waves from the tropics into the Northern Hemisphere extra-tropics (Webster 1982).
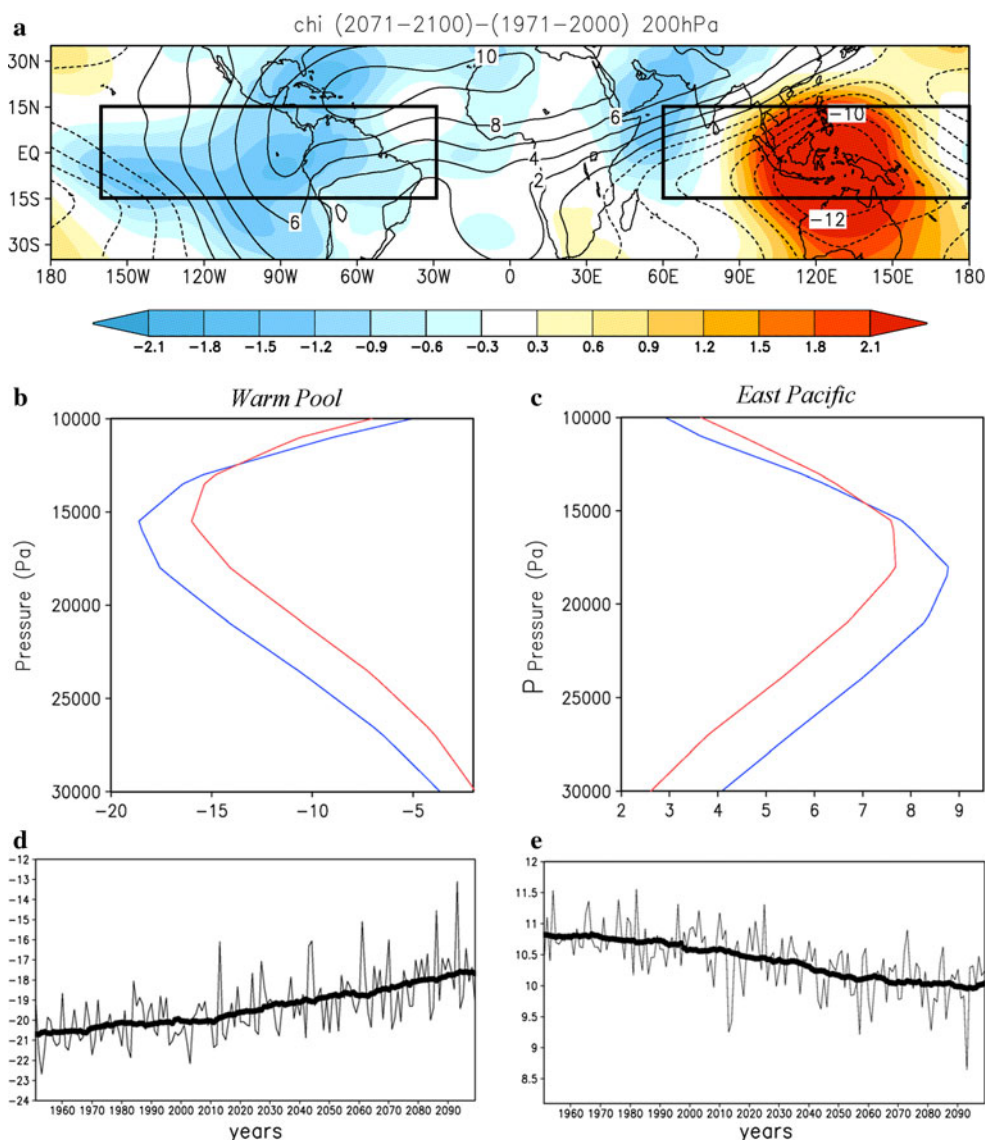
Fig. 3 Velocity potential (10^6 m^2 s^{-1}) of the ESSENCE ensemble mean. *Upper panel*: **a** *Shaded*: difference in velocity potential at 200 hPa between Future and Present period. *Contours*: present velocity potential at 200 hPa. *Middle panels*: *vertical* profile of the velocity potential averaged over warm pool (60–180°E, 15°S–15°N) (**b**) and East Pacific (160–30°W, 15°S–15°N) (**c**). Present: *blue curve*. Future: *red curve*. The warm pool and East Pacific are indicated by *boxes* in **a**. *Lower panels*: time evolution of the maximum of the profile of the velocity potential averaged over the warm pool (**d**) and East Pacific (**e**). The *thick lines* indicate 30-year running ensemble mean

4 Results

4.1 Anthropogenic changes of the Walker circulation

Figure 3 shows for the ESSENCE ensemble mean the change in the Walker circulation between Future and Present. The structure of the velocity potential χ shown here emphasizes the large scale structure of the Walker circulation; in the divergence (Fig. 4) it is masked by small scale structures due to the second order derivatives. Figure 3 (upper panel) clearly shows both the weakening of the rising branch over the West Pacific and the downward branch over the East Pacific. The vertical structure of χ over the warm pool and the cold tongue region shown in Fig. 3 (middle panels) reveals that also the vertical structure changes. Above 150 hPa χ does not decrease but instead slightly increases. The result is not only a reduction of the maximum of χ but also a squeezing and upward lifting of the vertical profile of χ. Figure 3 (lower panels) shows that for the ESSENCE ensemble mean the weakening of the Walker circulation is approximately linear in time similar as shown for the CMIP3 models in Fig. 1.

The change in the 200 hPa divergence D for the ESSENCE ensemble mean between the Future and Present

Fig. 4 Divergence (10^{-6} s^{-1}) of the ESSENCE ensemble mean in DJF. **a** Difference in divergence at 200 hPa between Future and Present period. **b** Divergence at 200 hPa for the Present period multiplied by −0.3. **c** Difference in divergence between 250 and 200 hPa for the Present period
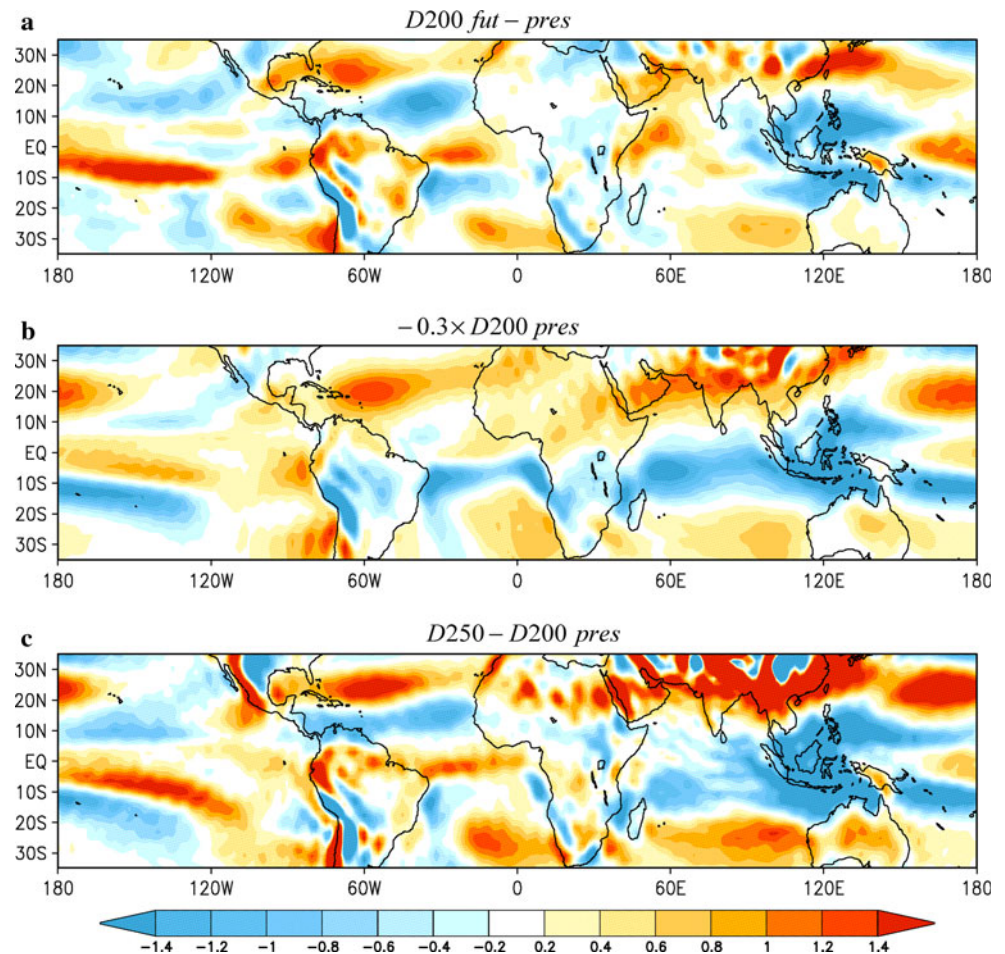
climate is shown in Fig. 4a. Figure 4b reveals that this change is similar to a uniform weakening of the divergence by about 30%. The largest deviations from a uniform reduction are over the Indian Ocean and the eastern Pacific. The pattern correlation between the Present 200 hPa D and its anthropogenic change is 0.51. The approximately uniform reduction of the Walker circulation due to greenhouse warming was also noted by Vecchi and Soden (2007) for the CMIP3 multimodel mean. Figure 3 (middle panels), however, shows that apart from a weakening there is also an upward shift of the Walker circulation. The difference between Future and Present 200 hPa divergence is therefore better approximated by the difference between the divergence at 250 and 200 hPa for the Present climate as shown in Fig. 4c and revealed by a larger pattern correlation of 0.70. Due to this lifting the Present 250 hPa D will become approximately the Future 200 hPa D. Figure 5a shows for the ESSENCE members the pattern correlation and ratio of the standard deviation between the anthropogenic change in upper tropospheric divergence and a 30% reduction in the Present upper tropospheric divergence (triangles) and upward shift of the 250 hPa divergence to 200 hPa (circles). It reveals moderate variability between

the different members, although a few members display substantially lower correlations indicating that even for a 30-year period there is significant intra-ensemble variability.

Figure 5b is similar as Fig. 5a but now for the CMIP3 models. It reveals significant correlations for a number of models. The average pattern correlation is, however, rather low 0.37. Comparison between Fig. 5a, b reveals that the spread between the CMIP3 models is larger than the spread between the different members of ESSENCE, indicating that the difference between the CMIP3 models is primarily due to differences in model formulation and not due to internal variability. Similar as for ESSENCE the correlations become larger if we take the difference between the divergence at 200 and 250 hPa for the Present climate. The average pattern correlation for the CMIP3 models increases to 0.55. The ratio of the standard deviation is about 0.7, revealing that for most models a significant part of the change in upper tropospheric divergence can be explained by a weakening and an upward shift of the Walker circulation. Figure 5b, however, also shows that there is a large spread among the CMIP3 models. Notable extremes are MIROCH with a correlation of 0.85 and GFDL21 with a
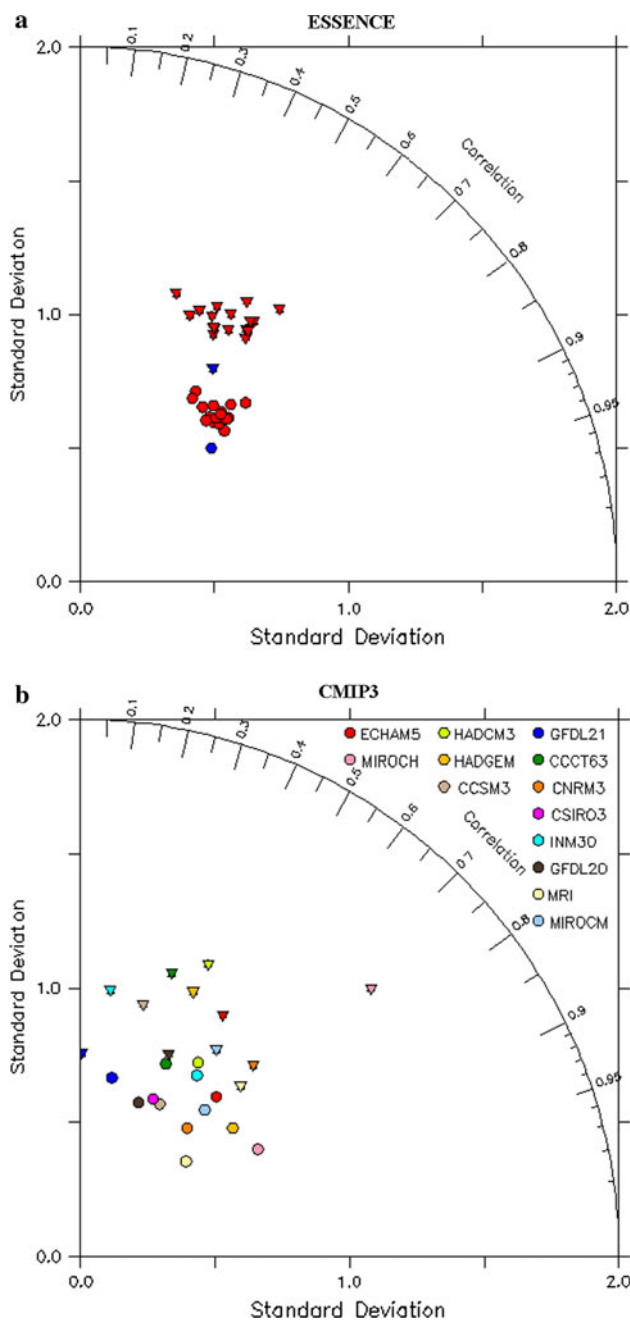
Fig. 5 a Taylor diagram comparing for ESSENCE the difference between Future and Present 200 hPa divergence in DJF with the difference between Present 200 and 250 hPa divergence (*circles*) and a 30% reduction in Present divergence (*triangles*). *Red*: individual ensemble members. *Blue*: ensemble mean. **b** As **a** but now for the CMIP3 models

correlation of 0.21. Interestingly these are also two models with respectively a large and small change in the upper tropospheric divergence. Because the Walker circulation is also affected by changes in SST and precipitation patterns we hypothesize that in case of a small reduction in the Walker circulation these factors will become more prominent.

Vecchi and Soden (2007) already have shown that an anthropogenic weakening of the Walker circulation is a robust signal in climate models and that the weakening of the Walker circulation is larger than the weakening of the Hadley circulation. They have shown this for the vertical velocity ω at 500 hPa. We have shown here that this weakening also induces a significant weakening of the upper tropospheric divergence. We hypothesize that this weakening of the upper tropospheric divergence will change the RWS and modify the generation of Rossby waves that propagate into the extra-tropics. This will be investigated in the next section.

4.2 Impact of anthropogenic changes in the Walker circulation on extra-tropical planetary waves

In this section we will investigate the impact of anthropogenic changes in the Walker circulation on the extra-tropical planetary waves using the BVE. As outlined in Sect. 2 the anthropogenic tropical forcing of the BVE can be computed directly by the RWS ΔS from the anthropogenic change in the upper tropospheric divergence and divergent wind of the climate models and indirectly by ΔF_{asym}^{trop}. We have computed the forcings ΔS and ΔF_{asym}^{trop}, and the responses of the BVE for all the individual model runs. The average of the CMIP3 models will be called the CMIP3 multi model mean and the average over the ESSENCE members the ESSENCE ensemble mean.

Figure 6a, b show ΔS and ΔF_{asym}^{trop} for the CMIP3 multi model mean. A large number of features in both patterns agree. However the amplitude of ΔS is much larger than of ΔF_{asym}^{trop} and had to be multiplied by 0.3 to obtain about the same amplitude of ΔF_{asym}^{trop} in Fig. 6. This is due to the fact that the circulation at 500 hPa is forced by the RWS over a layer in the upper troposphere and ΔS is computed for 200 hPa were it is maximal. In addition, although the extra-tropical response is equivalent barotropic the amplitude at 500 hPa is about 3 times smaller than the response at 200 hPa as shown in Fig. 2. In the simulations shown below ΔS is multiplied by 0.3. The similarity between ΔS and ΔF_{asym}^{trop}, which are computed independently, supports the assumption that the BVE is a suitable diagnostic tool for investigating the anthropogenic change of the extra-tropical planetary wave structure despite its shortcomings. It neglects for instance the feedbacks due to changes in the transient and stationary eddy forcing, and the nonlinear interaction with the topography. Because the BVE is a first order approximation of planetary Rossby wave propagation we do not expect exact agreement between ΔS and ΔF_{asym}^{trop}, but we do expect gross similarity in their structures and also in their extra-tropical responses. A similar agreement is observed between the ESSENCE ensemble mean ΔS and ΔF_{asym}^{trop} with a pattern correlation of

0.40 (not shown). As discussed in Sect. 4.1 there is apart from a weakening of the Walker circulation also an upward shift as shown in Fig. 3b. The upward shift might imply that the level of forcing of the Rossby waves also shifts upward. To test whether this affects our results we also computed ΔS averaged over the layer 300–100 hPa. For the multi-model mean the structure is very similar albeit weaker (It is still about 2 times stronger than ΔF_{asym}^{trop}) with a pattern correlation of 0.91 with ΔS computed at 200 hPa, indicating that for the Present as well as the Future climate the 200 hPa can be taken as the reference level for computing the RWS.

Figure 7 (upper panels) shows for the CMIP3 multi model mean the change in the meridional wind V between Future and Present climate and the simulation of this change by the BVE using ΔF_{asym}^{trop} and ΔS for the latitude band 30°S–30°N. Outside this latitude band the change in the forcing is zero. The change in V simulated by the CMIP3 multi model mean shows a circumglobal wave train with wave number 5 that strongly resembles the circumglobal wave guide pattern (CWP) described by Branstator (2002). The BVE forced with both ΔS and ΔF_{asym}^{trop} simulates a similar CWP pattern indicating that this wave train is forced from the tropics. The agreement of the CMIP3 multi model mean response with the BVE forced with ΔF_{asym}^{trop} is quite good with a pattern correlation of 0.64 for the latitudinal band 30°–90°N. All the correlations given below are for this latitudinal band. The agreement with the BVE forced with ΔS is somewhat less with a pattern correlation of 0.61. We expect a better agreement for ΔF_{asym}^{trop} because by construction the BVE reproduces the response exactly when the total ΔF is

used. ΔF_{asym}^{trop} accounts for the imperfections of the BVE, whereas ΔS is a pure approximation of the forcing of Rossby waves propagating from the tropics into the extra-tropics. The discrepancy is largest over the Pacific for both ΔF_{asym}^{trop} and ΔS. Over the Atlantic and Europe the agreement is rather good. Also the change of V in the ESSENCE ensemble mean has a similar CWP pattern (not shown) that can also be approximately simulated by the BVE forced with ΔS and ΔF_{asym}^{trop} with a pattern correlation of 0.45 and 0.71 respectively.

These results confirm the conclusion of Selten et al. (2004) and Branstator and Selten (2009) that the anthropogenic change of the CWP is forced from the tropics. In addition these results indicate that the forcing of the extra-tropical planetary Rossby waves can be effectively modeled by the change in the RWS that is dominated by the weakening of the Walker circulation.

The tropics are defined here as the region between 30°S and 30°N. Figure 7 reveals that part of the response is within this latitude band, which makes the notion of an extra-tropical response generated by a tropical forcing less clear. Narrowing the tropical belt to 20°S–20°N for the RWS strongly deteriorates the response for the extra-tropics. This can be understood because the RWS in Fig. 6 attains significant amplitudes poleward of 20°. The RWS is dominated by the stretching term which vanishes close to the equator due to the dependence of f on latitude. One may note, however, that there is still a significant response in V poleward of 30° and remind that all the correlations computed above are for the region poleward of 30°. From this we argue that a significant source of the extra-tropical change in V resides in the tropics.

Fig. 6 **a** Ensemble mean difference of the Rossby Wave Source ΔS (10^{-11} s^{-2}) at 200 hPa for DJF between Future and Present for the CMIP3 multi model mean under the SRES A1B scenario. **b** As **a** but now for ΔF_{asym}^{trop}. In **a** ΔS is multiplied with 0.3 (see text for explanation)
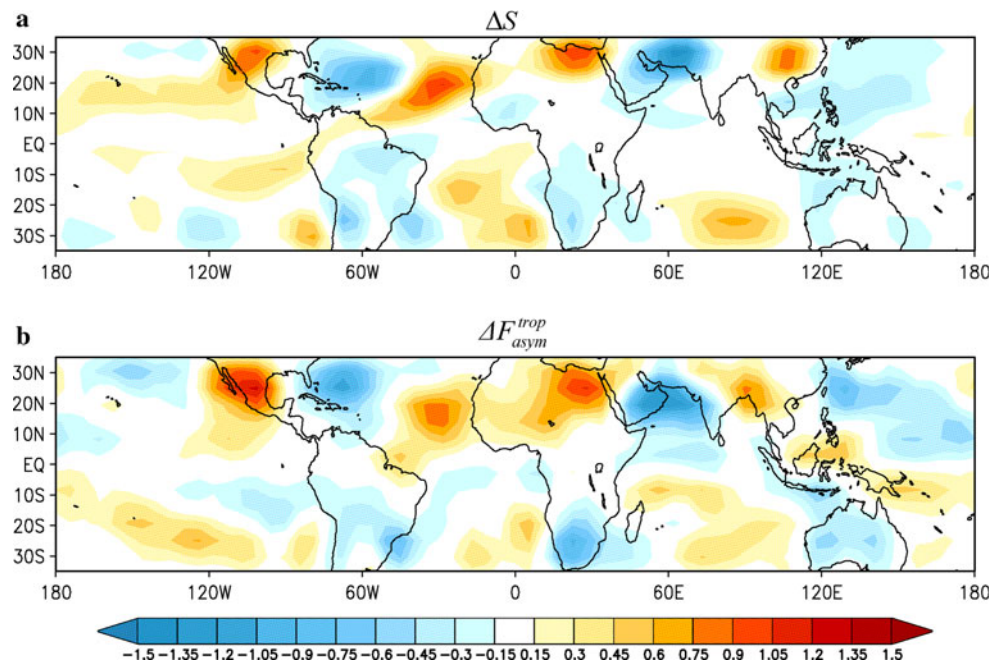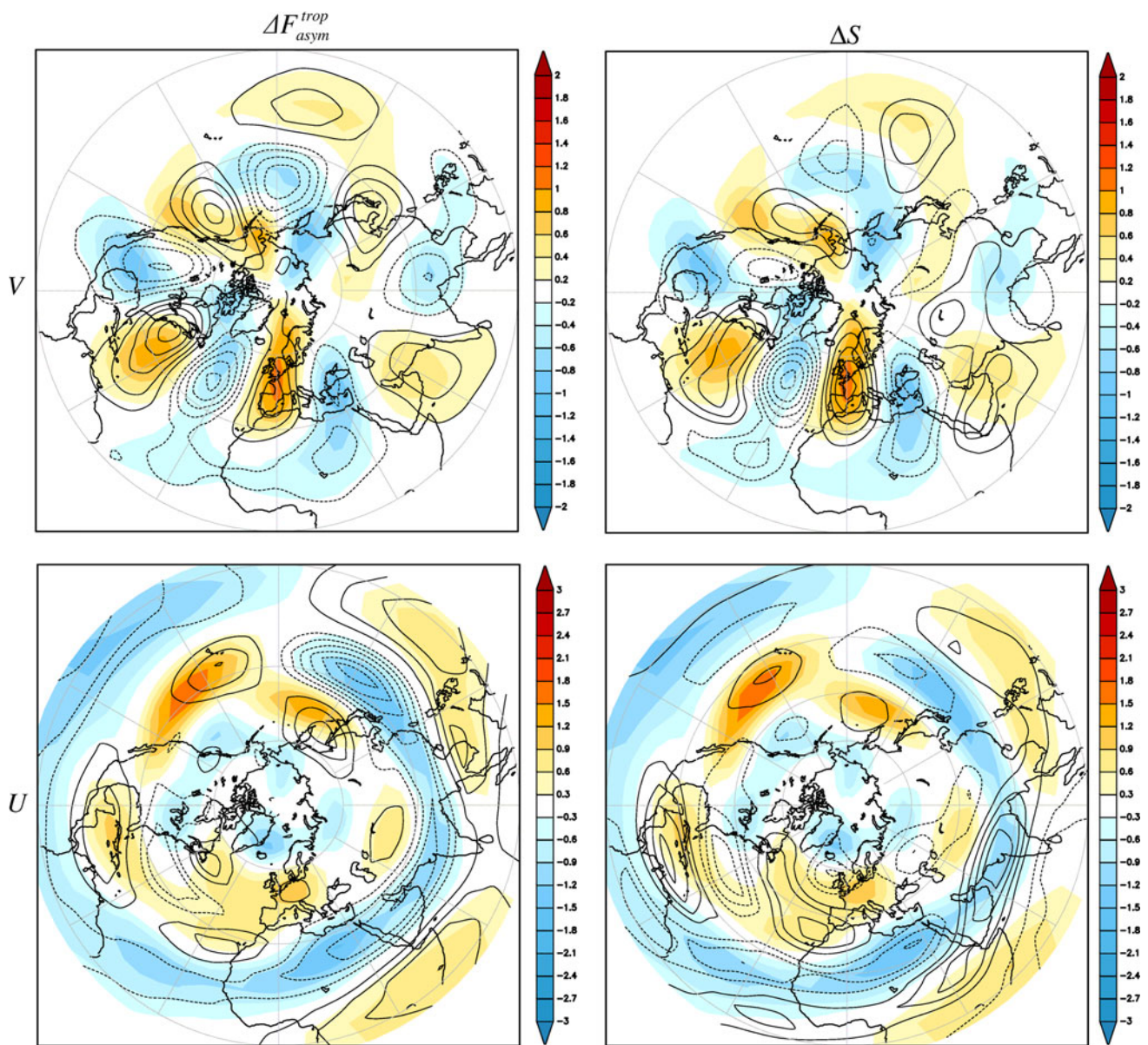
Fig. 7 *Shaded*: ensemble mean change in *V* (*upper panels*) and *U* (*lower panels*) (m s^{-1}) at 500 hPa between 2071–2100 and 1971–2000 for DJF simulated by the CMIP3 multi model mean under the SRES A1B scenario. Units in (m s^{-1}). *Contours*: change in *V* (*contour* interval 0.2 m s^{-1}, zero *contour* omitted) and *U* (*contour* interval 0.3 m s^{-1}, zero *contour* omitted) simulated by the BVE with asymmetrical tropical forcing ΔF_{asym}^{trop} (*left panels*) and ΔS (*right panels*)

Figure 8 shows that there is substantial variation in the ability of the BVE to simulate the anthropogenic change in V in the different CMIP3 models. Notable negative outliers are GFDL21 and HADGEM with correlations of 0.3 and 0.4 for ΔF_{asym}^{trop}. MIROCH and CCSM3 on the other hand reveal correlations of nearly 0.8. Further inspection revealed that GFDL21 and HADGEM did not show a clear CWP pattern dominated by wave number 5. In general models with a clear CWP pattern showed the largest correlations. Figure 8 also reveals that the amplitude of the signal forced by the asymmetrical tropical forcing is very

small for the GFDL21 model further suggesting that for the GFDL21 model changes in the planetary wave structure are not forced by changes in the tropics.

The results for the individual ESSENCE members are also shown in Fig. 8. The correlations are generally lower than for the ESSENCE ensemble mean and display a considerable spread, varying between 0.8 and 0.4 for ΔF_{asym}^{trop} and between 0.6 and 0.2 for ΔS. There is also substantial variation in the amplitude of extra-planetary wave response as shown in Fig. 8. Visual inspection of the response patterns of V reveals that most members did
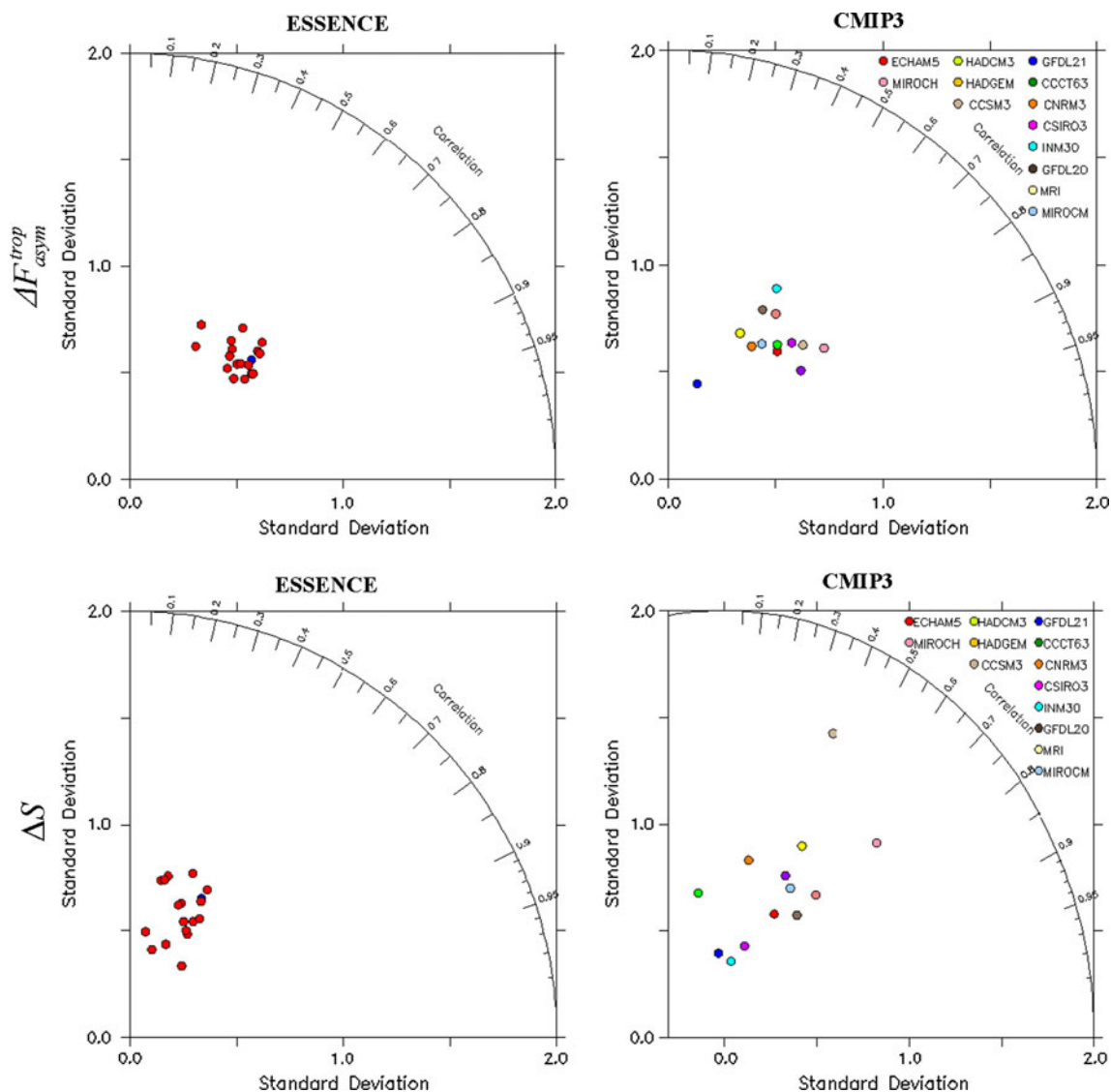
Fig. 8 Taylor diagrams comparing the extra-tropical anthropogenic change in V simulated by the climate model and approximated by BVE using ΔF_{asym}^{trop} (*upper panels*) and ΔS (*lower panels*). *Left panels*: ESSENCE. *Right panels*: CMIP3 models

generate the CWP pattern but that for a few members this was less clear. These were also the members for which the change was less explained by changes in the asymmetrical tropical circulation. Although there is considerable spread within the ESSENCE ensemble, it is less in comparison with the CMIP3 models in agreement with the smaller spread in the divergence shown in Fig. 5. This once more stresses the observation that the spread due to the model formulation is larger than due to internal variability. The differences between the CMIP3 models are primarily due to their model formulation and are not so much affected by internal variability.

The change in zonal wind U is shown in Fig. 7 (lower panels). South of 30°N the agreement between the CMIP3 multi model mean and the BVE forced with ΔF_{asym}^{trop} is rather good, which is no surprise because we have specified

the forcing of the BVE for that region. The zonal mean component in the tropical forcing that is omitted here is apparently not of crucial importance. North of 30°N the agreement between the BVE and CMIP3 multi model mean is less although the BVE captures to some extend the meridional shift in U. The pattern correlation for the Northern Hemisphere between 30 and 90°N is 0.41. The agreement between the CMIP3 multi model mean and the BVE forced with ΔS is, similar as for V, less with a pattern correlation of 0.30.

5 Discussion

In the foregoing section we have shown that the weakening of the Walker circulation has a significant impact on the

extra-tropical planetary wave structure in particular on the meridional wind V. The impact on the zonal wind U appears to be weaker. Here we will discuss the role and impact of other factors of the climate system that potentially might affect the planetary wave structure response in a warmer climate, like a shift in the zonal mean circulation, mid-latitude forcing and tropical SST. In addition we will discuss the importance of simulating correctly the present-day extra-tropical planetary wave structure and the regional deviations from an uniform weakening and upward shift of the Walker circulation. We will also discuss the impact on the extra-tropical planetary wave-structure of tropical forcings in different longitudinal sections. Finally we will discuss the role of critical lines and the topography.

5.1 Impact of change of zonal mean forcing

Apart from the weakening of the Walker circulation, the weakening and widening of the Hadley circulation is also a robust anthropogenic change (Lu et al. 2007, 2009; Reichler and Held 2005; Seidel et al. 2008). In addition outside the tropics the CMIP3 models simulate a shift in the zonal mean circulation that appears to be related to changes in transient eddy activity (Lu et al. 2009). Brandefelt and Körnich (2008) showed for the CMIP3 models a significant impact of the changes in the zonal mean wind on the planetary wave structure. To compare the impact of the changes in the Walker circulation to the impact of a shift of the zonal mean circulation we forced the BVE with the change in the zonal mean forcing [ΔF] including the tropics. The change in V simulated by the BVE for the CMIP3 multi model mean is small. The ratio of the standard deviation is 0.42 and the pattern correlation 0.33 (not shown). Similar values are obtained for the ESSENCE ensemble mean (0.32 and 0.45 respectively). It suggests that the impact of the change in zonal mean flow on V is small and negligible compared to the impact of the asymmetrical tropical forcing. The impact on U is larger as shown in Fig. 9 for the CMIP3 multi model mean. It captures the global pole ward meridional shift in U and to some extend the local maxima and minima. The pattern correlation is 0.49 for the CMIP3 multi model mean and 0.55 for the ESSENCE ensemble mean.

Brandefelt and Körnich (2008) grouped the models into three different groups according to the shape of the stationary wave response. They obtained pattern correlations of the stream function due to the change in the zonal mean flow for each of these groups of 0.71, 0.61 and 0.21. The pattern correlations that we obtained for the stream function patterns are 0.45 for the CMIP3 multi model mean and 0.56 for the ESSENCE ensemble mean. These pattern correlations fall within the range obtained by Brandefelt and Körnich, suggesting that the simulated changes in the

stream function by Brandefelt and Körnich (2008) are dominated by the changes in U with a negligible contribution from V.

5.2 Role of mid-latitude forcing

To compare the impact of mid-latitude forcing with the tropical forcing we calculated the response to the extra-tropical part of ΔF, $\Delta F^{extra-trop}$ (30°–90°N), which is shown in Fig. 10a. It reveals a rather small scale structure with the largest amplitudes mainly over the oceans. In the Present as well as the Future climate F is a representation of processes that are not represented explicitly in the BVE such as the effect of orography, transient and stationary waves and atmosphere–surface interactions. These processes all contribute to the stationary wave response, with possible cancellation between them (Ting et al. 2001; Held et al. 2002). The contribution of the different terms is yet unclear. Stephenson and Held (1993) found that the transient eddies dominate the total anthropogenic response, on the other hand using the same model at higher resolution Joseph et al. (2004) show that the zonal mean changes have a comparable contribution as the zonally asymmetric forcing, including transients and diabatic heating. Only a decomposition of $\Delta F^{extra-trop}$ would reveal the relevance of the different contributions, which is outside the scope of this paper.

The impact of $\Delta F^{extra-trop}$ on V is substantial as shown in Fig. 10b. The response has its largest amplitude at the northern latitudes, where the agreement with the CMIP3 model mean is very good. For the CMIP3 multi model mean the pattern correlation is 0.62 and the ratio of the standard deviation is 0.75 which is comparable with 0.64 and 0.89 for ΔF^{trop}_{asym}. If we separate the response between the southern and northern part of the extra-tropics then the correlation for ΔF^{trop}_{asym} becomes 0.70 and 0.49 for 30°–60°N and 60°–90°N respectively and for $\Delta F^{extra-trop}$ 0.49 and 0.90. This confirms that in the southern part of the extra-tropics the response is dominated by the forcing from the tropics, whereas in the northern extra-tropics it is dominated by the mid-latitude asymmetrical forcing.

Figure 10c shows that the impact on U is large with significant contributions over the storm track regions where we expect the largest impact of the transient eddies. Over these regions the agreement with the simulated changes by the CMIP3 multi model mean is good. The pattern correlation is 0.81 and the ratio of the standard deviation is 0.84, suggesting that for the anthropogenic change in the zonal wind U the asymmetrical extra-tropical forcing is the most dominant factor, although also the zonally asymmetrical tropical forcing also makes a significant contribution (Fig. 7, pattern correlation 0.41).

Fig. 9 *Shaded*: ensemble mean change in U (m s^{-1}) at 500 hPa between Future and Present for DJF simulated by CMIP3 multi model mean under the SRES A1B scenario. *Contours*: change in U (*contour* interval 0.3 m s^{-1}, *zero contour* omitted) simulated by the BVE forced with the zonal mean forcing [ΔF]
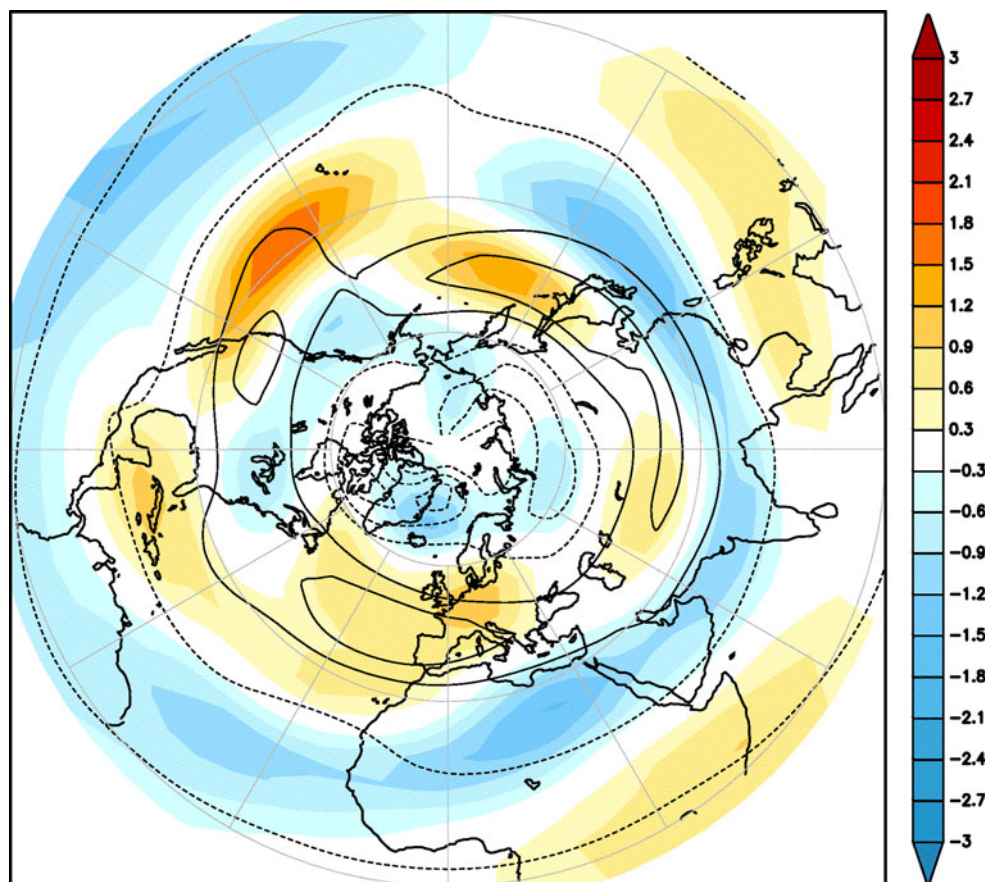
5.3 Role of tropical SSTs

The interannual variability of extra-tropical planetary waves is significantly affected by tropical SST anomalies. Especially El-Niño has a large extra-tropical impact, but also smaller tropical SST anomalies in other ocean basins do affect the extra-tropical planetary wave structure. It is therefore natural to assume that the anthropogenic change in tropical SST will affect the extra-tropical planetary wave structure. Indeed there are number of studies (e.g. Selten et al. 2004; Hoerling et al. 2001; Shin and Sardeshmukh 2010) that argue that Future changes in the tropical SST will affect the planetary wave structure. The basic mechanism how tropical SST will affect the RWS is that tropical SST will affect the diabatic heating Q. In the tropics there is approximately a balance between diabatic heating and adiabatic cooling by upward motion $\sigma\omega = -Q/c_p$. Using this balance and the continuity equation $\nabla \cdot \vec{V} = -\partial\omega/\partial p$ the anomalous divergence $\hat{D}$ is given by

$$\hat{D} = \frac{\partial}{\partial p}\left(\hat{Q}/\sigma c_p\right)$$

Most of the diabatic heating in the tropics generated by SST anomalies is due to the release of latent heat. For interannual variability there is therefore a clear relationship between SST anomalies, precipitation anomalies and anomalous RWS (Held and Kang 1987).

Figure 11a–c show for the ESSENCE ensemble mean the change between Future and Present climate for SST, precipitation and 200 hPa divergence respectively. For the SST the area mean value has been subtracted in order to highlight the asymmetric changes. Significant increase in precipitation is observed along the inter tropical convergence zone (ITCZ) especially over the Pacific and Indian Ocean, with an accompanying increase in the divergence. The impact on the RWS is, however, small (see Fig. 6a) because the RWS is dominated by the fD term and the planetary vorticity f vanishes at the equator. Figure 11 does not reveal a direct relationship between changes in tropical SST with either changes in precipitation or the divergence. Tropical SST does affect the circulation but the induced changes also modify the SST which obscures the relationship.

5.4 Importance of correctly simulating the climatological planetary waves

The impact of the tropical forcing on the extra-tropical planetary wave structure not only depends on the tropical
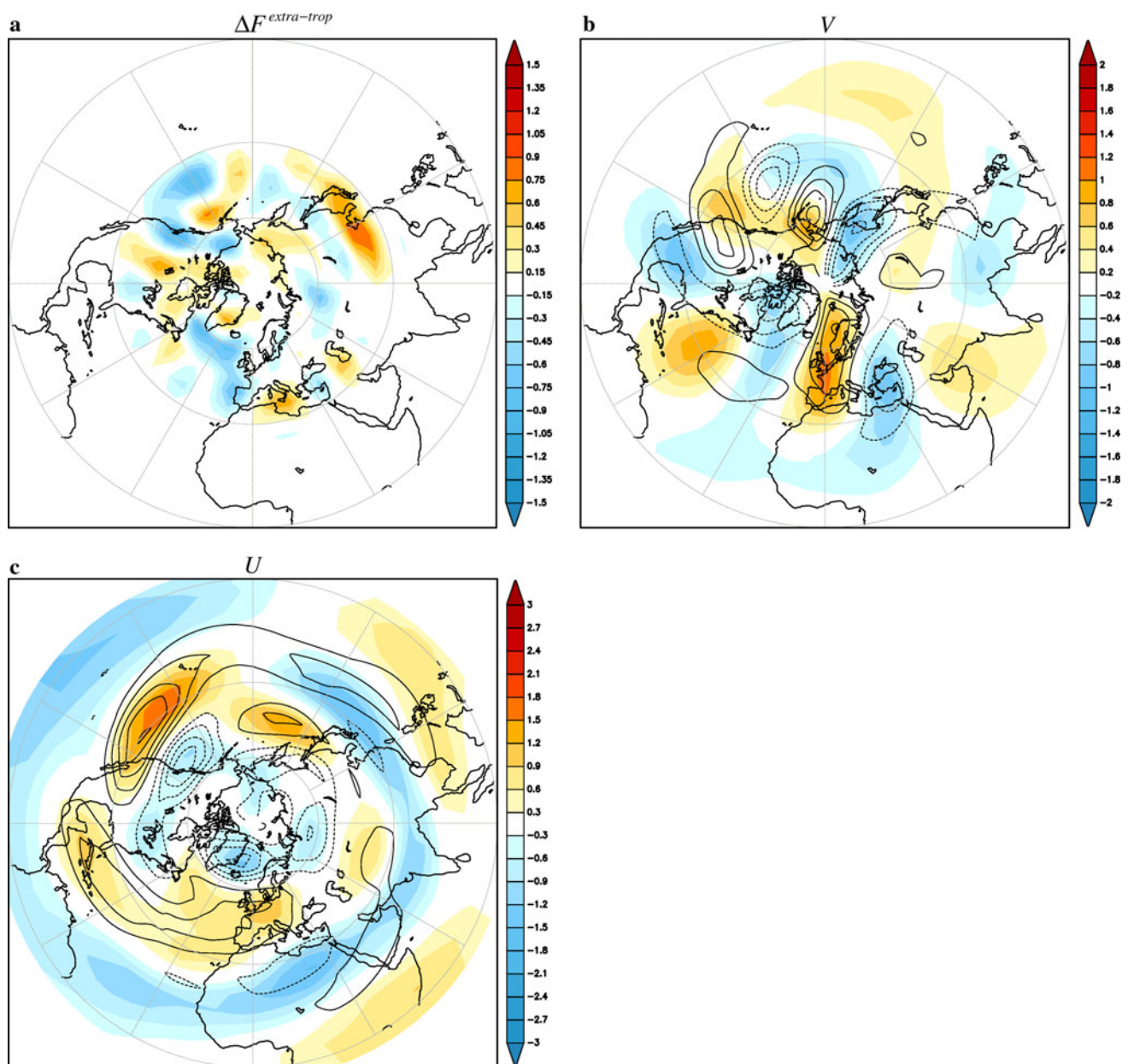
Fig. 10 a Difference in extra-tropical forcing (30°–90°N) of the BVE between Future and Present for DJF ($\Delta F^{extra-trop}$) computed for the CMIP3 multi model mean (10^6 s^{-2}). **b** *Shaded*: CMIP3 multi model change in meridional wind V (m s^{-1}) between at 500 hPa between 2071–2100 and 1971–2000 for DJF. *Contours* change in V (*contour interval* 0.2 m s^{-1}, *zero contour* omitted) simulated with the BVE forced with the extra-tropical forcing $\Delta F^{extra-trop}$. **c** As **b** but now for zonal wind U (*contour interval* 0.3 m s^{-1}, *zero contour* omitted)

forcing itself but also on the propagation characteristics of Rossby waves that depend on to the climatological mean state. To investigate this latter effect we again applied ΔS of the CMIP3 models at the BVE but now using the 'observed' ERA40 climatology, instead of the simulated climatology, as the climatological mean state of the BVE. Table 2 shows for V the pattern correlation with the original experiments using the simulated climatological stream function. For the majority of models the pattern correlation is larger than 0.8 (0.91 for the CMIP3 multi model mean) indicating that the differences between the CMIP3 models in the extra-tropical planetary wave response are primarily due to differences in the simulated changes in the Walker circulation and not due to differences in the simulated climatological planetary wave pattern. The two models that have pattern correlations substantially below 0.8 (GFDL21 0.57 and CSIRO3 0.65) are also two models for which the amplitude of the

Fig. 11 ESSENCE ensemble mean in DJF. **a** Difference in SST (°C) between Future and Present. The tropical area mean (30°S–30°N) change in SST has been subtracted. **b** Difference in precipitation (mm day^{-1}) between Future and Present. **c** Difference in 200 hPa divergence (10^{-6} s^{-1}) between Future and Present
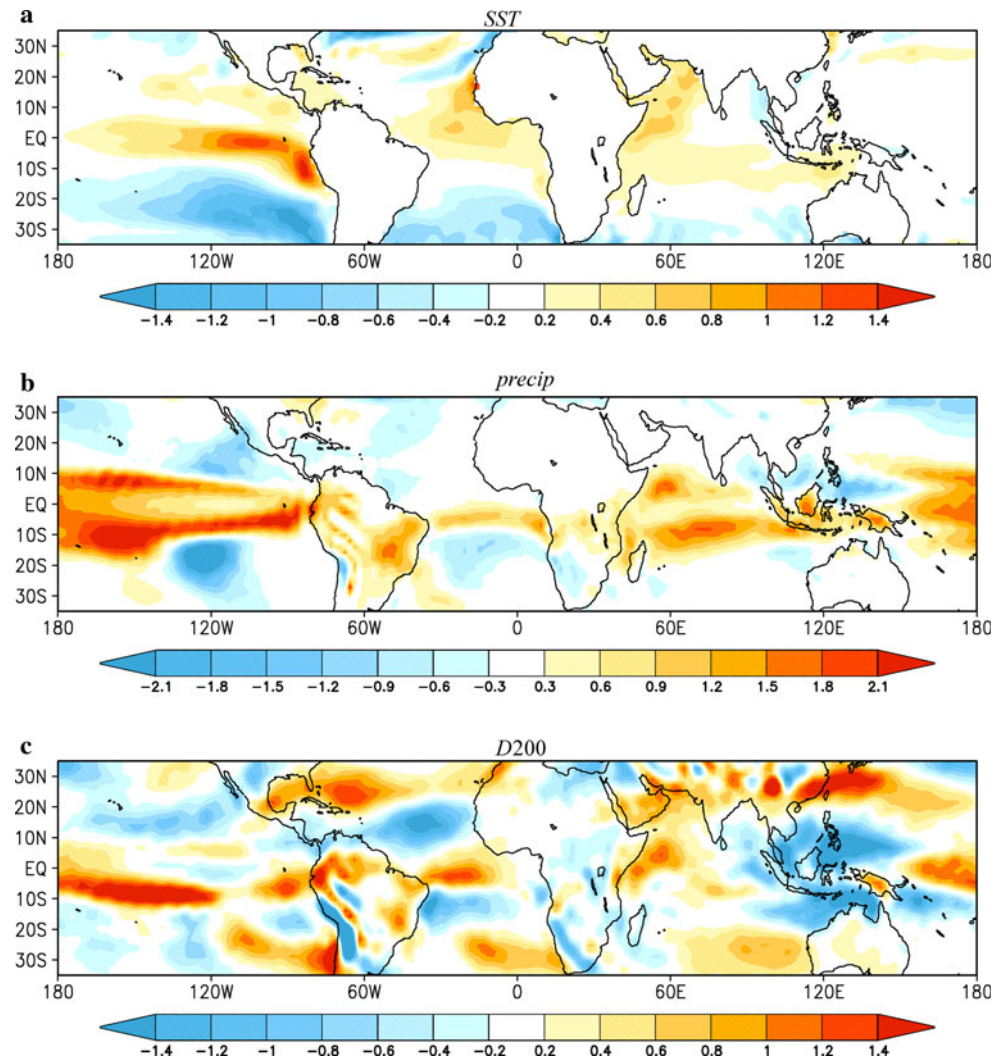
response is small, which is due to the small ΔS. The small signal due to the small forcing is likely masked by the internal variability of the model.

5.5 Impact of deviations from uniform weakening of Walker circulation

The dominant anthropogenic changes of the Walker circulation are the weakening and the upward shift. It is tempting to investigate whether the anthropogenic changes in the extra-tropical planetary wave circulation can be simply computed from a uniform reduction or upward shift of the Walker circulation. In Fig. 12 we show for the CMIP3 multi model mean the planetary wave response simulated with the BVE where we have computed the RWS from a 30% uniform weakening of the 200 hPa divergence (Fig. 12a) or the upward shift of the Present 250 hPa divergence to 200 hPa divergence (Fig. 12b). The

patterns correlations with the planetary wave structure simulated by the BVE with the original RWS ΔS are 0.78 and 0.67 respectively. This indeed shows that to a large extend the anthropogenic changes in the extra-tropical planetary wave structure are due to a reduction and upward shift of the Walker circulation. On the other hand these pattern correlations are sufficiently different from unity to argue that not only should the Present Walker circulation be simulated well but that a correct simulation of the extra-tropical planetary wave structure also crucially depends on a correct simulation of the anthropogenic changes in the Walker circulation in amplitude as well as structure. This is illustrated by the drop in the pattern correlation for V between the CMIP3 multi model mean and the BVE forced with ΔS from 0.61 to 0.38 for the BVE forced with the RWS computed from a 30% reduction and to 0.35 for BVE forced with the RWS computed from the upward shift of the Walker circulation.

Table 2 Pattern correlation for the AR4 IPPC models between the response patterns in V simulated with the BVE forced with ΔS using their own Present climatological state and the ERA40 basic state

CMIP3 model	Pattern correlation
ECHAM5	0.84
HADCM3	0.75
GFDL21	0.57
MIROCH	0.76
HADGEM	0.91
CCCT63	0.89
CCSM3	0.85
CNRM3	0.83
CSIRO3	0.65
INM30	0.80
GFDL20	0.79
MRI	0.85
MIROCM	0.88

5.6 Impact of regional changes in the Walker circulation

Although the impact of tropical SST, by modifying the RWS, on the extra-planetary waves for interannual variability has been demonstrated by numerous studies, it was also noted that this influence does not extend to all regions. For instance the impact of El-Niño on the extra-tropical circulation over a remote area such as Western Europe is rather weak (van Oldenborgh et al. 2000). Branstator (2002) on the other hand showed that the subtropical jet

can act as a waveguide and that for certain forcing regions this results in a remote response. He identified the CWP pattern as a global pattern that can be effectively locally forced. Because many CMIP3 models show a response pattern in V that is similar to this CWP it raises the question if there are preferred regions for generating this response. To investigate this we divided for the ESSENCE ensemble mean, which shows a clear CWP pattern, the asymmetrical tropical forcing in 8 longitudinal sectors of $45°$, starting at $0°$. For each of these sectors we computed the response to the change in asymmetrical tropical forcing. Figure 13 shows for the ESSENCE ensemble mean the results of the sector forcings of ΔF_{asym}^{trop}. It reveals that the forcing limited to sectorial regions has a regional impact. A downstream response is observed but the longitudinally extent is generally less than $90°$. The largest responses are at the jet entrances of the Pacific and Atlantic jet. Each of these responses projects significantly on the CWP pattern which therefore stands out as the resulting global response. The sector responses can be added linearly resulting in a response that is equal to the global response (not shown).

5.7 Stationary wave reflection by the critical line

Planetary waves excited in the mid latitudes propagate to the low latitudes. There they are absorbed and reflected at the critical line where the phase speed of the wave matches the background zonal wind. Changes in the excitation of the extra-tropical planetary waves and/or the reflection properties at the critical line might therefore also
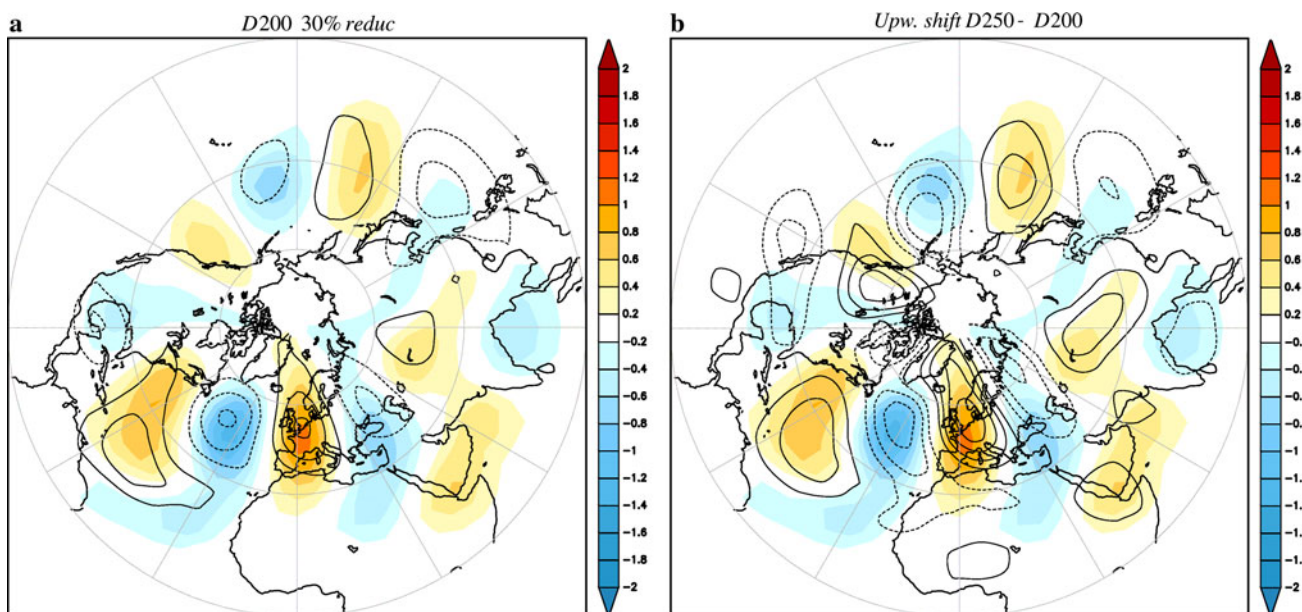

Fig. 12 CMIP3 multi model mean. **a** *Contours*: simulated response in V (m s^{-1}) of the BVE forced by the RWS that is computed for a 30% reduction of the Present 200 hPa divergence. **b** *Contours*: same as **a** but now for the upward shift of the 250 hPa divergence to 200 hPa. The *shaded colors* in **a** and **b** show the response in V of the BVE forced by the RWS ΔS

affect the planetary wave structure (Brunet and Haynes 1996; Walker and Magnusdottir 2003). Much of the changes in upper tropospheric divergence (Fig. 4) and the RWS (Fig. 6) are situated poleward of the critical line. These changes could therefore also partly be generated by changes in the reflection of stationary waves at the critical line. At this moment we are unable to separate this mechanism from a weakening of the Walker circulation. However, the large agreement in structure between the Present upper tropospheric divergence and its change (Fig. 4), suggests that the weakening of the Walker circulation plays an important role.

The reflection of waves at the critical line is a small scale process, especially in meridional direction, that is not well resolved by a T21 horizontal resolution. Therefore we redid the analysis for ESSENCE with a higher resolution of T42. The results are very similar clearly showing the wave number 5 response (not shown). The pattern correlations for ΔF_{asym}^{trop} and ΔS are 0.56 and 0.68, which is comparable to 0.45 and 0.71 for the T21 resolution. This further supports the notion that reflection at the critical line does not play a crucial role in explaining the change in the planetary wave structure simulated by the CMIP3 models. In addition, although the simulated change of V in ESSENCE shown in

Fig. 13 (shaded) suggests that reflection at the critical line might play a role, this is not supported by the regional responses (Fig. 13 contours). They all follow a great circle path and are damped before they approach the critical line.

5.8 Topography

The climatological planetary wave structure is to a large extend forced by the topography. Nonlinear interactions between the atmospheric circulation and the topography might therefore contribute to Future changes in the planetary wave structure. The impact of topography should be investigated with a three-dimensional model. However, as a first approximation of the topographic effect we have included the topography as an extra forcing in the BVE, similar as in Källen (1981). In Källen the topography is included by vertically integrating the BVE, assuming the atmosphere to be equivalent barotropic and taking the vertical velocity at the surface to be given by $\omega_0 = -g\rho_0 \vec{V} \cdot \nabla m$, where m is the dimensional mountain height. This introduces an extra term in the Jacobian: $J(\psi, \xi + f + h)$, where $h = f_0 A(p_0) \frac{m}{H}$. Here f_0 is the coriolis parameter at $45°$, $A(p)$ the vertical structure of the stream function and H the scale height of the troposphere. p_0 is
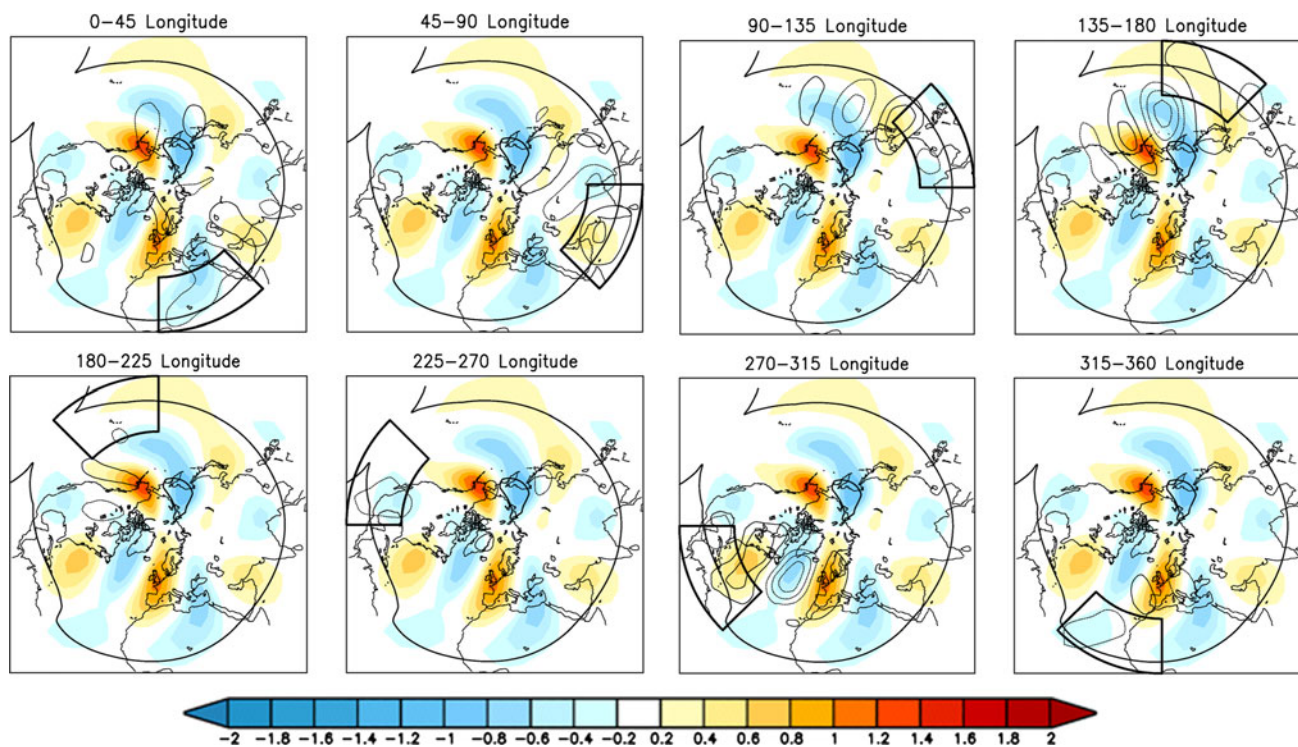

Fig. 13 ESSENCE ensemble mean. *Contours*: Simulated change in V (m s^{-1}) by the BVE due to forcing of ΔF_{asym}^{trop} over sectors of $45°$ longitude, starting with the sector $0–45°$. *Contour interval 0.2 m s^{-1}, zero contour is omitted. The black box indicates the forcing area.

Shaded: simulated change in V in DJF by the ESSENCE ensemble mean. The *thick black line* indicates the zero wind line (U = 0) in the Present climate
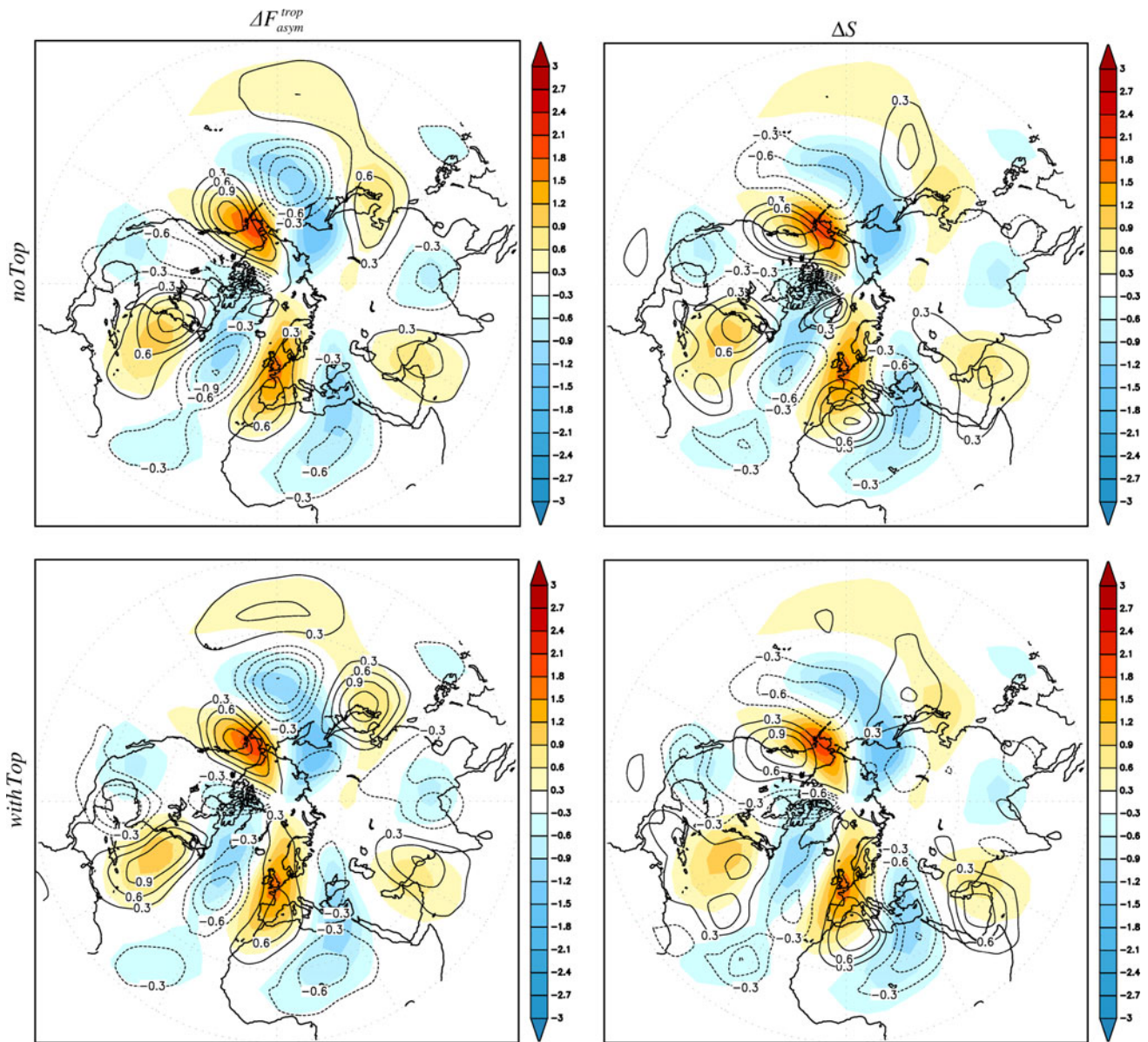
Fig. 14 *Shaded*: ensemble mean change in V (m s^{-1}) at 500 hPa between 2071–2100 and 1971–2000 for DJF simulated by ESSENCE under the SRES A1B scenario. Units in (m s^{-1}). *Contours*: change in V (*contour* interval 0.3 m s^{-1}, *zero contour* omitted) simulated by the BVE with asymmetrical tropical forcing. *Upper panels*: BVE without topography, *lower panels*: BVE with topography. *Left panels* ΔF_{asym}^{trop}, *right panels* ΔS

surface pressure. For a detailed derivation see Källen (1981), where he estimates $A(p_0) = 0.5$ and $H = 8$ km.

With the modified BVE we have estimated for ESSENCE the effect of topography. The inclusion of the topography has only a minor effect on the response to the tropical forcings ΔF_{asym}^{trop} and ΔS as shown in Fig. 14. The main conclusions are not altered. The dominant response in V is still the circumglobal wave number 5 response that agrees well with the simulated change in V.

Apart from a weakening the Hadley circulation widens in response to anthropogenic warming. This induces a shift

in the zonal mean flow that affects the planetary wave structure by interaction with the topography. We have investigated this with the BVE by computing the response to the simulated change in the zonally averaged stream function. The response is weak and does not show a wave number 5 pattern (not shown). The pattern correlation is very low: 0.24. Although we recognize that the impact of topography can only be fully investigated with a model that resolves the vertical structure of the atmospheric circulation, the results of this preliminary study, in agreement with Joseph et al. (2004), do not point toward a dominant role of the topography.
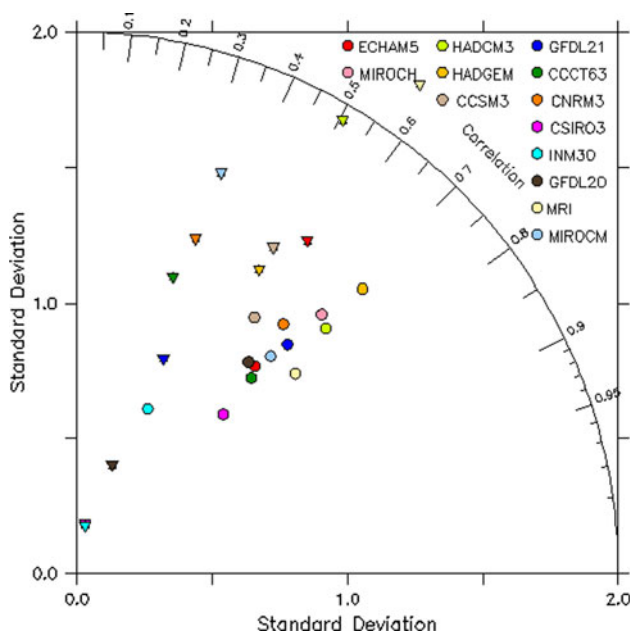
Fig. 15 Taylor diagram comparing CMIP3 models with ERA-interim. *Circles*: 200 hPa divergence in DJF (30°N–30°S). *Triangles*: difference between 200 and 250 hPa divergence in DJF (30°N–30°S)

6 Conclusions

The weakening of the Walker circulation appears to be a robust aspect of anthropogenic climate change in CMIP3 models. One of the consequences of this weakening is a reduction of the upper tropospheric divergence. The CMIP3 climate models that we investigated here simulate a reduction in the order of 20–30% at the end of this century under an SRES A1B scenario. In addition to this reduction there is an upward shift. As a result of the weakening and upward shift of the upper tropospheric divergence the forcing of Rossby waves propagating from the tropics into the extra-tropics is affected altering the extra-tropical planetary wave structure.

Using the BVE as a diagnostic tool we have shown that the extra-tropical planetary wave structure is significantly modified by these anthropogenic changes in the Walker circulation. The dominant pattern in the CMIP3 anthropogenic planetary wave response is the CWP pattern although large inter-model variability is observed. The CWP pattern with wave zonal wave number 5 is most clearly seen in the meridional wind V. The relative impact of the weakening of the Walker circulation on the zonal wind U is less. The large impact of the weakening of the Walker circulation on the planetary-wave structure implies that for a reliable simulation of the anthropogenic changes in the planetary-wave structure a correct simulation of the present day Walker circulation is crucial.

This raises the question how well the CMIP3 models simulate the Walker circulation and in particular the upper

tropospheric divergence. The best data sets presently available for the upper tropospheric divergence are the ERA-interim and NCEP re-analysis data sets. One should however realize that the divergence in those reanalysis is affected by the model formulation and its possible deficiencies. Comparison between ERA-interim and NCEP should give some indication of the quality upper tropospheric divergence in those data sets because these reanalysis are computed with different models. For the NCEP data we have computed the upper tropospheric data over the same period as ERA-interim. The pattern correlation between the ERA-interim and NCEP reanalysis is 0.84, suggesting that we can use these re-analyses to evaluate the quality of the upper tropospheric divergence simulated by the CMIP3 models.

The pattern correlation between the 200 hPa divergence of the CMIP3 models and ERA-interim is shown in Fig. 15. For most models the pattern correlation is around 0.7, although there is substantial variation among the CMIP3 models, indicating that although the basic structures are well represented by the models there are still significant deficiencies. Not surprisingly the vertical structure in the upper tropospheric divergence is less well simulated with correlations between the simulated and observed (200–250 hPa) difference fields varying between 0.1 and 0.6. One should note however that the agreement between ERA-interim and NCEP is also rather poor with a pattern correlation of 0.6.

The significant deficiencies in the simulation of the present day Walker circulations implies that improvements in the simulation of the Walker circulation of present day state-of-the-art climate models are essential for producing more reliable estimates of anthropogenically induced changes of the extra-tropical planetary wave structure.

References

Brandefelt J, Körnich H (2008) Northern Hemisphere stationary waves in future climate projections. J Clim 21:6341–6353. doi:10.1175/2008JCLI2373.1

Branstator GW (2002) Circumglobal teleconnections, the jet stream waveguide, and the North Atlantic Oscillation. J Clim 15:1893–1910

Branstator GW, Selten FM (2009) Modes of variability and climate change. J Clim 22:2639–2658

Brunet G, Haynes PH (1996) Low-latitude reflection of Rossby wave trains. J Atmos Sci 53:482–496

Dee DP et al (2011) The ERA-interim reanalysis: configuration and performance of the data assimilation system. Q J R Meteorol Soc 137:553–597

Déqué M et al (2007) An intercomparison of regional climate simulations for Europe: assessing uncertainties in model projections. Clim Change 81:53–70. doi:10.1007/s10584-006-9228-x

Haarsma RJ, Opsteegh JD (1989) Nonlinear response to anomalous tropical forcing. J Atmos Sci 46:3240–3255

Haltiner GJ (1971) Numerical weather prediction. Wiley, London. ISBN:0-471-34580-6

Held IM, Kang I-S (1987) Barotropic models of the extra-tropical response to El Niño. J Atmos Sci 44:3576–3586

Held IM, Soden BJ (2006) Robust responses of the hydrological cycle to global warming. J Clim 19:5686–5699

Held IM, Lee Panetta R, Pierrehumbert RT (1985) Stationary external Rossby waves in vertical shear. J Atmos Sci 42:865–883

Held IM, Ting M, Wang H (2002) Northern winter stationary waves: theory and modeling. J Clim 15:2125–2144

Hoerling MP, Hurrell JW, Xu T (2001) Tropical origins for recent North Atlantic climate change. Science 292:90–92

Hoskins BJ, Ambrizzi T (1993) Rossby wave propagation on a realistic longitudinally varying flow. J Atmos Sci 50:1661–1671

Hoskins BJ, Karoly DJ (1981) The steady linear response of a spherical atmosphere to thermal and orographic forcing. J Atmos Sci 38:1179–1196

Joseph R, Ting T, Kushner PJ (2004) The global stationary wave response to climate change in a coupled GCM. J Clim 17:540–556

Källen E (1981) The nonlinear effects of orographic and momentum forcing in a low-order, barotropic model. J Atmos Sci 38:2150–2163

Kalnay E et al (1996) The NCEP/NCAR 40-year reanalysis project. Bull Am Meteorol Soc 77:437–471

Lu J, Vecchi GA, Reichler T (2007) Expansion of the Hadley cell under global warming. Geophys Res Lett 34:L06805. doi:10.1029/2006GL028443

Lu J, Deser C, Reichler T (2009) Cause of the widening of the tropical belt since 1958. Geophys Res Lett 36:L03803. doi:10.1029/2008GL036076

Meehl GA, Covey C, Taylor KE, Delworth T, Stouffer RJ, Latif M, McAvaney B, Mitchell JFB (2007) The WCRP CMIP3 multi-model dataset. Bull Am Meteorol Soc 88:1383–1394

Reichler TJ, Held IM (2005) Evidence for a widening of the Hadley cell. 17th AMS conference on climate. Variability and change. American Meteorological Society, Cambridge

Sardeshmukh PD, Hoskins BJ (1985) Vorticity balances in the tropics during the 1982–83 El Niño-Southern Oscillation event. Q J R Meteorol Soc 111:261–278

Seidel DJ, Fu Q, Randel WJ, Reichler TJ (2008) Widening of the tropical belt in a changing climate. Nat Geosci 1:21–24

Selten FM, Branstator GW, Dijkstra HA, Kliphuis M (2004) Tropical origin for recent and future Northern Hemisphere climate change. Geophys Res Lett 31:L21205. doi:10.1029/2004GL020739

Shin S-I, Sardeshmukh PD (2010) Influence of Tropical Ocean warming on remote climate trends. Clim Dyn. doi:10.1007/s00382-009-0732-3

Solomon S, Qin D, Manning M, Chen Z, Marquis M, Averyt KB, Tignor M, Miller HL (2007) Climate change 2007: the physical science basis. Cambridge University Press, Cambridge

Stephenson DB, Held IM (1993) GCM response of northern winter stationary waves and storm tracks to increasing amounts of carbon dioxide. J Clim 6:1859–1870

Sterl A, Severijns C, Dijkstra H, Hazeleger W, van Oldenborgh GJ, van den Broeke M, Burgers G, van den Hurk B, van Leeuwen PJ, van Velthoven P (2008) When can we expect extremely high surface temperatures? Geophys Res Lett 35:L14703. doi:10.1029/2008GL034071

Ting M, Wang H, Yu L (2001) Nonlinear stationary wave maintenance and seasonal cycle in the GFDL R30 GCM. J Atmos Sci 58:2331–2354

Uppala S et al (2005) The ERA-40 re-analysis. Q J R Meteorol Soc 131:2961–3012

van Oldenborgh GJ, Burgers G, Klein Tank A (2000) On the El-Niño teleconnection to spring precipitation in Europe. Int J Climatol 20:565–574

van Ulden AP, van Oldenborgh GJ (2006) Large-scale atmospheric circulation biases and changes in global climate model simulations and their importance for climate change in Central Europe. Atmos Chem Phys 6:863–881

Vecchi GA, Soden BJ (2007) Global warming and the weakening of the tropical circulation. J Clim 20:4316–4430

Vecchi GA, Soden BJ, Wittenberg AT, Held IM, Leetmaa A, Harrison MJ (2006) Weakening of tropical Pacific atmospheric circulation due to anthropogenic forcing. Nature 441:73–76

Verkley WTM (1987) Stationary barotropic modons in westerly background flows. J Atmos Sci 44:2383–2398

Walker CC, Magnusdottir G (2003) Nonlinear planetary wave reflection in an atmospheric GCM. J Atmos Sci 60:279–286

Webster PJ (1982) Seasonality in the local and remote atmospheric response to sea surface temperature anomalies. J Atmos Sci 39:41–52

Woollings T (2010) Dynamical influences on European climate: an uncertain future. Philos Trans R Soc A 368:3733–3756